Applied Catalysis B: Environmental 165 (2015) 20–26

Contents lists available at ScienceDirect

Applied Catalysis B: Environmental

journal homepage: www.elsevier.com/locate/apcatb

Photo-oxidation activities on Pd-doped TiO_2 nanoparticles: critical PdO formation effect

Hangil Lee [a], Minjeong Shin [a], Myungjin Lee [a], Yun Jeong Hwang [b,*]

[a] Department of Chemistry, Sookmyung Women's University, Seoul 140-742, Republic of Korea
[b] Clean Energy Research Center, Korea Institute of Science and Technology, Seoul 136-791, Republic of Korea

ARTICLE INFO

Article history:
Received 22 July 2014
Received in revised form
22 September 2014
Accepted 24 September 2014
Available online 2 October 2014

Keywords:
$PdTiO_2$ nanoparticles
Photocatalytic oxidation
Raman Spectroscopy
HRPES
PdO.

ABSTRACT

The catalytic activities of three distinct Pd-doped TiO_2 ($PdTiO_2$) nanoparticle samples, post-annealed (at 700, 800, and 900 °C) after fabrication on silicon substrates, were analyzed with respect to the photo-oxidation of aniline and 2-thiophenecarboxaldehyde. Through a combination of Raman spectroscopy and high-resolution photoemission spectroscopy (HRPES), we demonstrated that the photocatalytic oxidation occurred only when the $PdTiO_2$ nanoparticles were annealed at temperatures above 800 °C, that is, when PdO and Ti^{3+} had partially formed on the $PdTiO_2$ nanoparticles, which indicates that the presence of PdO and Ti^{3+} is critical for the photocatalytic oxidation. Additionally, we determined the decrease in the band gaps to visible region with $PdTiO_2$ nanoparticles annealed above 800 °C from their valence-band spectra, which resulted in photocatalytic activities even under visible light, $\lambda = 540$ nm.

1. Introduction

In recent decades, many researchers have intensively investigated the chemical properties of TiO_2 substrates and nanostructures because of their various applications such as solar cells, catalysis, gas sensing, medical implantation, corrosion protection, etc. [1–3]. The catalytic activity of TiO_2 is enhanced in nanostructures with large specific surface areas, which exhibit improved catalytic efficiencies. However, the practical applications of TiO_2 are limited by its poor light absorption in the visible region, due to its large band gap (E_g = 3.0–3.2 eV), and its poor efficiency in catalytic reactions, many of which are known to occur only in the presence of oxygen vacancies on the TiO_2 surface [4,5].

There have been many attempts to overcome these limitations; one of the most popular approaches is the introduction of foreign elements as dopants. The band gap of TiO_2 can be narrowed from UV to the visible region by introducing various elements, especially transition metals or anions [6,7]. Furthermore, the catalytic reactivity of TiO_2 can be enhanced by doping which controls various properties including defects, electronic band structures and carrier concentrations, etc. [8,9].

$PdTiO_2$ nanoparticles are expected to exhibit a reduced band gap and improved catalytic activity. In this study, we systematically investigated the photocatalytic activities of three distinct $PdTiO_2$ nanoparticle samples with respect to the oxidations of aniline and 2-thiophenecarboxaldehyde (TPCA), which are difficult to oxidize under normal conditions and have N and S atoms in the functional group, respectively. The photocatalytic reactions between these molecules and molecular oxygen (O_2) were characterized when PdO was present on the $PdTiO_2$ nanoparticle surfaces. We concluded that post-thermal treatment at temperatures above 800 °C produces PdO and Ti^{3+} on the nanoparticle surfaces, which significantly influence the optical and photocatalytic properties and result in enhanced activities. To our knowledge, there has been no previous systematic experimental study of the role of PdO presence on the enhanced photocatalytic activity with TiO_2.

2. Experimental

2.1. $PdTiO_2$ nanoparticles preparation

$PdTiO_2$ nanoparticles were fabricated with a co-sputtering method from a circular polycrystalline TiO_2 sample (99.99%, diameter: 2 in.) and Pd targets (99.999%, diameter: 2 in.). The base pressure of the deposition chamber was approximately 1×10^{-6} Torr, and the working process pressure was approximately 2×10^{-3} Torr. Pure argon gas (99.999%) was used as an inert gas in

* Corresponding author. Tel.: +82 2 958 5227; fax: +82 2 958 5809.
E-mail address: yjhwang@kist.re.kr (Y.J. Hwang).

http://dx.doi.org/10.1016/j.apcatb.2014.09.061
0926-3373/

the chamber. We performed co-depositions of Pd and TiO_2 targets on Si substrates by using the RF and DC magnetron sputtering techniques, respectively, at room temperature. The argon plasma for the Pd and TiO_2 depositions was applied at RF powers of 200 W and DC 100 W, respectively. We adjusted the size of the $PdTiO_2$ nanoparticles to a thickness of 50 nm. The resulting $PdTiO_2$ nanoparticles were annealed in a tube furnace at the desired temperature (700, 800, or 900 °C) under Ar conditions for 12 h.

2.2. Oxidation reactions

Aniline ($C_6H_5NH_2$; Sigma Aldrich, 99.9%) and 2-thiophenecarboxaldehyde (2-C_4H_3SCHO; TPCA, Sigma Aldrich, 99.0%) were purified by turbo pumping to remove impurities prior to dosing onto the $PdTiO_2$ nanoparticles. A direct dozer controlled by means of a variable leak valve was used to dose onto the $PdTiO_2$ nanoparticles grown on silicon substrates. The pressure of the chamber was 10^{-6} Torr during dosing, and the amount of the exposed aniline and TPCA molecules were varied by the dosing time from 0 to 36 min to become 0–2160 L (Langmuir). During the co-exposure of the two molecules and molecular oxygen, we exposed the system to UV (λ = 365 nm, VL-4.LC Tube 1 × 4 W, Vilber Loumat) or visible (λ = 540 nm, Ultra-Bright Green LED Penlight, 13–15 W) light to enhance the catalytic reactions.

2.3. Characterization

The morphologies of the samples were characterized by performing field-emission scanning electron microscopy (FE-SEM, JEOL JSM-7600F) at an acceleration voltage of 15 kV and field-emission transmission electron microscopy (FE-TEM, JEOL JEM-2100F(HR)) at an accelerating voltage of 200 kV. The chemical states of doped Pd were determined with a home-built Raman spectroscope equipped with an Ar^+ ion laser (Spectra-Physics Stabilite 2017) as an excitation source, a spectrometer (HORIBA Jobin Yvon TRIAX 550), and a CCD detector (HORIBA Jobin Yvon Symphony) cooled to 140 K. The wavelength of the incident excitation beam was 514.5 nm. HRPES experiments were performed at the 8A2 beamline at the Pohang Accelerator Laboratory (PAL), which was equipped with an electron analyzer (SES100, Gamma-Data Scienta). The Ti 2p, Pd 3d, N 1s, S 2p, and O 1s core-level spectra were obtained by using photon energies of 510, 400, 460, 230, and 590 eV, respectively, to enhance the surface sensitivity. The binding energies of the core-level spectra were determined with respect to the binding energies (E_B = 84.0 eV) of the clean Au 4f core level for the same photon energy. Valence-band spectra and secondary electron cut-off spectra (−10 V sample bias) were measured at photon energies of 80 eV to measure the changes in the band gap and work function. All spectra were recorded in the normal emission mode. The photoemission spectra were carefully analyzed by using a standard nonlinear least-squares fitting procedure with Voigt functions [10].

3. Results and discussion

We first acquired SEM images and the corresponding Raman spectra of the $PdTiO_2$ nanoparticles prepared under three different conditions (Fig. 1). As the post-annealing temperature increased from 700 to 900 °C, the size of the $PdTiO_2$ nanoparticles increased. In the $PdTiO_2$ post-annealed at 700 °C ($PdTiO_2$-700), no separation

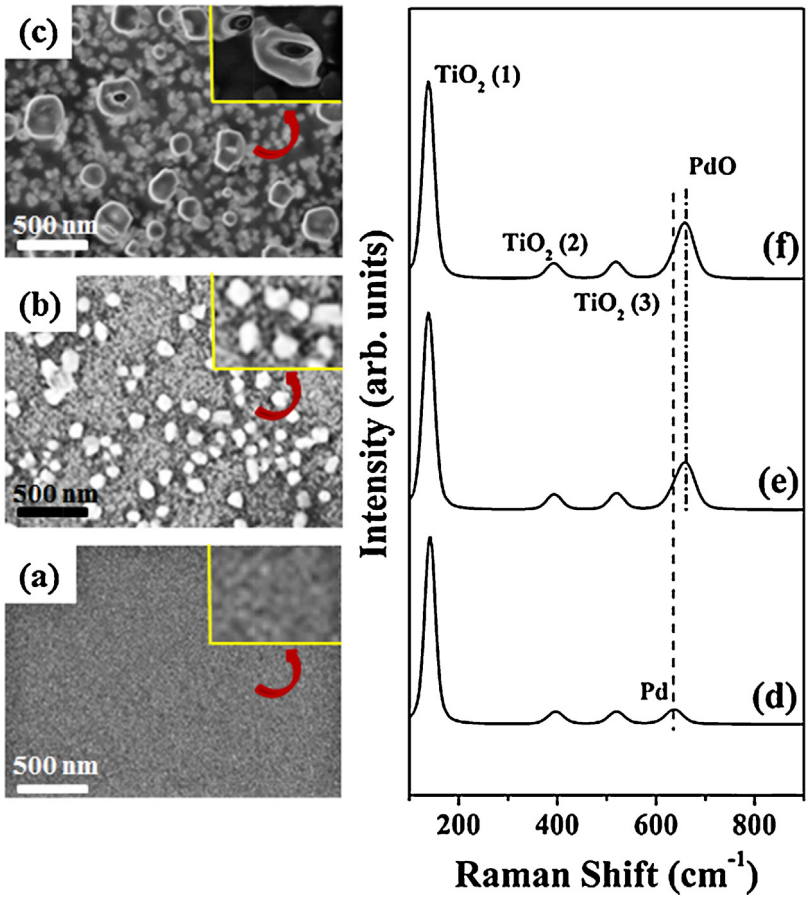

Fig. 1. SEM images and the corresponding Raman spectra, which show that the morphologies and chemical states of Pd vary as a result of annealing at temperatures above 800 °C. (a, d) Obtained from $PdTiO_2$-700, (b, e) from $PdTiO_2$-800, and (c, f) from $PdTiO_2$-900.

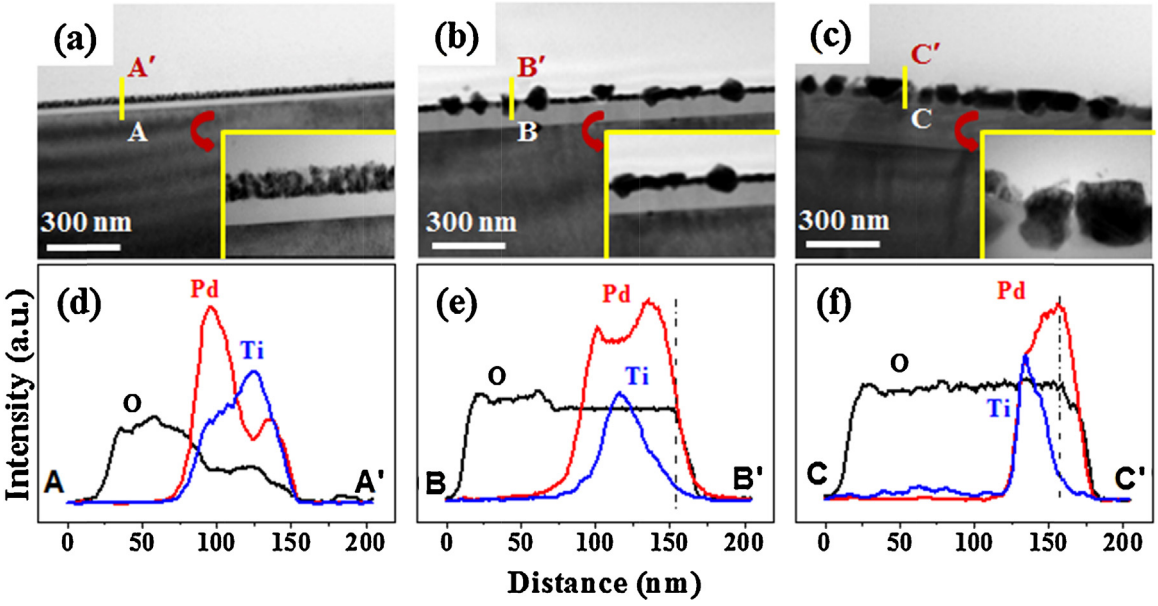

Fig. 2. TEM images, HRTEM images (insets), and EDX line mappings: (a, d) With $PdTiO_2$-700, (b, e) with $PdTiO_2$-800, and (c, f) with $PdTiO_2$-900.

of Pd from the TiO_2 nanoparticles was evident; note that the co-deposited Pd and TiO_2 are distributed homogeneously without any agglomeration. In contrast, the surface morphologies of the $PdTiO_2$ samples after post annealing at 800 °C ($PdTiO_2$-800) and 900 °C ($PdTiO_2$-900) are rougher due to the formation of large Pd (or PdO) particles on the surfaces of the $PdTiO_2$ nanoparticles, possibly due to the discrepancy between the surface free energies of Pd (~2.0 J/m^2) and TiO_2 (~1.7 J/m^2) [11,12].

In addition, a transition from Pd to PdO was observed by Raman spectroscopy as the post-annealing temperature increased (Fig. 1d–f). The Raman shift at 636 cm^{-1} indicated the presence of typical metallic Pd (Fig. 1d) [13], showing metallic Pd and TiO_2 can coexist without special hybridization after post-annealing at 700 °C, whereas the PdO-induced Raman shifts at 662 cm^{-1} was observed for the samples annealed at 800 and 900 °C [14]. Thus, critical changes in the surface morphology and chemical state from metallic Pd to PdO were obtained when the post-annealing temperature increased from 700 to 800 °C.

We also obtained cross-sectional TEM images of the three different $PdTiO_2$ nanoparticle samples (Fig. 2). $PdTiO_2$-700 was homogeneously distributed with a similar particle size at a depth of 75 nm. In contrast, the TEM images of $PdTiO_2$-800 and $PdTiO_2$-900 showed relatively large particles on the sample surfaces, as indicated by the SEM images. The EDX elementary line mappings show

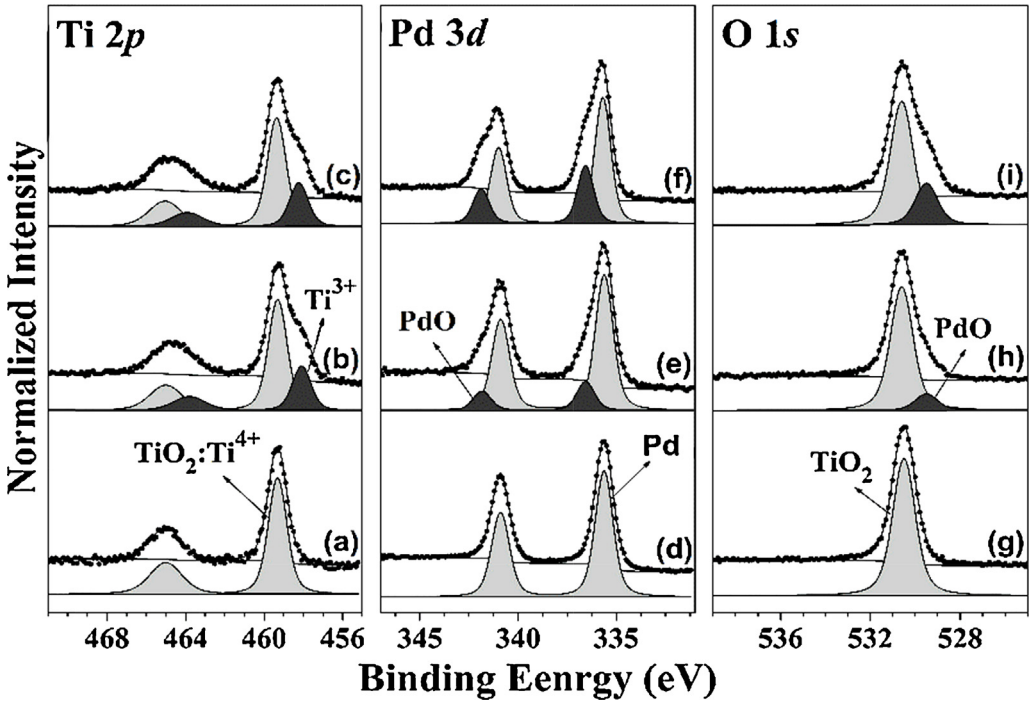

Fig. 3. HRPES results for the Ti 2p, Pd 3d, and O 1s core-level spectra of the $PdTiO_2$ nanoparticles annealed at various temperatures: (a, d, and g) core-level spectra from $PdTiO_2$-700; (b, e, and h) those from $PdTiO_2$-800; (c, f, and i) those from $PdTiO_2$-900.

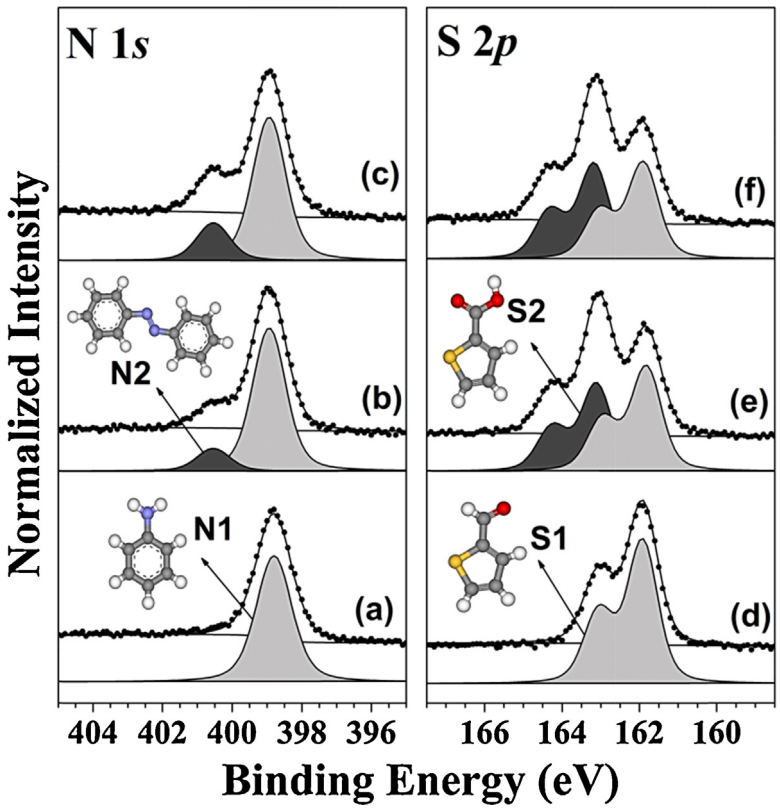

Fig. 4. HRPES results for the N 1s core-level spectrum and the S 2p core-level spectrum obtained from the various $PdTiO_2$ nanoparticles: core-level spectra after adsorption (a) and (d) onto $PdTiO_2$-700, (b, e) onto $PdTiO_2$-800, (c, f) onto $PdTiO_2$-900.

that the relative amounts of Pd and O near the top of the surface increase when the post-annealing temperature increased to 800 and 900 °C (Fig. 2d–f). This result is in good agreement with the Raman spectra in Fig. 1 and the HRPES data in Fig. 3.

The core-level spectra (Ti 2p, Pd 3d, and O 1s) of the $PdTiO_2$ nanoparticles were obtained with HRPES (Fig. 3) to determine the changes in the electronic properties. The concentration of Pd was 3.0% on average from the Pd 3d to Ti 2p peak ratio in the sampling depth of the HRPES measurement (not shown here). For $PdTiO_2$-700, each of the core-level spectra contains an independent single feature without any hybridization between Pd and TiO_2. The binding energies of the Ti 2p, Pd 3d, and O 1s core-level peaks were found to be 459.3, 335.5, and 530.6 eV, respectively; the binding energies and peak shapes indicate the presence of pure unmixed Pd and TiO_2 particles [15,16]. In contrast, $PdTiO_2$-800 and $PdTiO_2$-900 spectra contained additional bonding peaks. These spectra all contain two distinctive features: Ti 2p at 459.3 eV (Ti^{4+}) and 458.0 eV (Ti^{3+}), Pd 3d at 335.5 eV (Pd^0) and 336.5 eV (Pd^{2+}), and O 1s at 530.6 eV (TiO_2) and 529.5 eV (PdO), which clearly indicates the partial mixing of the Pd and TiO_2 particles. Increasing the post-annealing temperatures resulted in the partial transformation from metallic Pd to PdO and the Ti^{3+} electronic state (458.0 eV) simultaneously. Ti^{3+} species are also known to be related to oxygen vacancy states in TiO_2 because of charge compensation. These removed oxygen atoms from TiO_2 are considered to use to form PdO because the post-annealing was conducted in Ar condition.

Next, the photocatalytic activities of $PdTiO_2$ nanoparticles were compared by performing oxidation reactions on their surfaces with the molecules, aniline and TPCA, which are generally known to be difficult to oxidize. The surface-sensitive N 1s and S 2p core-level spectra were recorded by using HRPES after 360 L of aniline (Fig. 4a–c) and 360 L of TPCA (Fig. 4d–f) were deposited onto the $PdTiO_2$ nanoparticles, respectively, in the presence of the same amount of oxygen under 365 nm UV light illumination. Fig. 4a and d shows the N 1s core-level spectrum (due to aniline, labeled N1) and S 2p core-level spectrum (due to TPCA, labeled S1) obtained after adsorption onto $PdTiO_2$-700, respectively. Only non-oxidized peaks, a single N 1s peak at 398.8 eV associated with aniline [17] and a single S 2p peak at 161.9 eV associated with TPCA were observed [18,19], even though we deposited these molecules in the presence of oxygen and UV light source.

In contrast, both these molecules are oxidized on $PdTiO_2$-800 and $PdTiO_2$-900. The appearance of two distinct nitrogen peaks, one due to aniline (labeled N1, at 398.8 eV) and one due to azobenzene (labeled N2, at 400.6 eV), indicates that oxidation has occurred on the surfaces of $PdTiO_2$-800 and $PdTiO_2$-900. Similarly, there are two distinct sulfur peaks, one due to TPCA (labeled S1, at 161.9 eV) and one due to 2-thiophenecarboxylic acid (2-TCA, 2-C_4H_3SCOOH) (labeled S2, at 163.1 eV), which shows that oxidation from TPCA to 2-TCA has occurred [20]. These results demonstrate that the presence of PdO and Ti^{3+} on $PdTiO_2$-800 and $PdTiO_2$-900 facilitates the oxidations of aniline to azobenzene and TPCA to 2-TCA.

To investigate the influence of post-annealing on the electronic band structures of the $PdTiO_2$ nanoparticles, we recorded the valence-band spectra to determine the band gap shifts and measured the secondary electron cut-offs to quantify the changes in work function. As shown in the valence-band spectra (Fig. 5a–c), the band gap decreases from 2.85 to 2.24 eV and then to 1.92 eV as the post-annealing temperature increased from 700 to 800 °C and then to 900 °C. The decrease in the band gap can be explained by the increment of Pd (or PdO) particles on the surface of the $PdTiO_2$ nanoparticles during post-annealing at high temperatures, as occurs for doping with other transition metals [21,22]. Ti^{3+} species which were also observed with high-temperature annealed $PdTiO_2$ samples can absorb visible light as well by introducing surface states between conduction and valence band states [23].

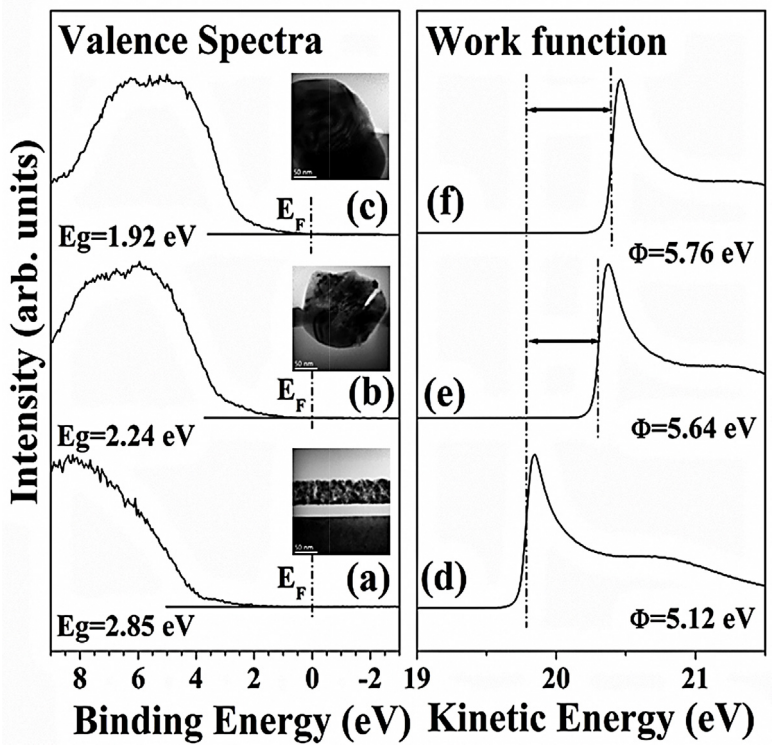

Fig. 5. (Left panel) Valence-band spectra and (right panel) work function changes (−20 V sample bias) obtained from the secondary electron cut-offs with a photon energy of 80 eV: (a, d) for $PdTiO_2$-700, (b, e) for $PdTiO_2$-800, (c, f) for $PdTiO_2$-900.

The work functions of the $PdTiO_2$ samples were also determined by locating the centers of the secondary electron cut-offs (Fig. 5d–f). The work function values of Pd (PdO) and TiO_2 are 5.12 eV (~7.9 eV) and 5.10 eV, respectively. The measured work function of $PdTiO_2$-700 was 5.12 eV, close to that of pure TiO_2 (5.10 eV) [24–26]. However, the higher work function at 5.76 eV was measured with $PdTiO_2$-900, in which the population of Pd on the surface increased due to the migration of Pd to the surface. Shift

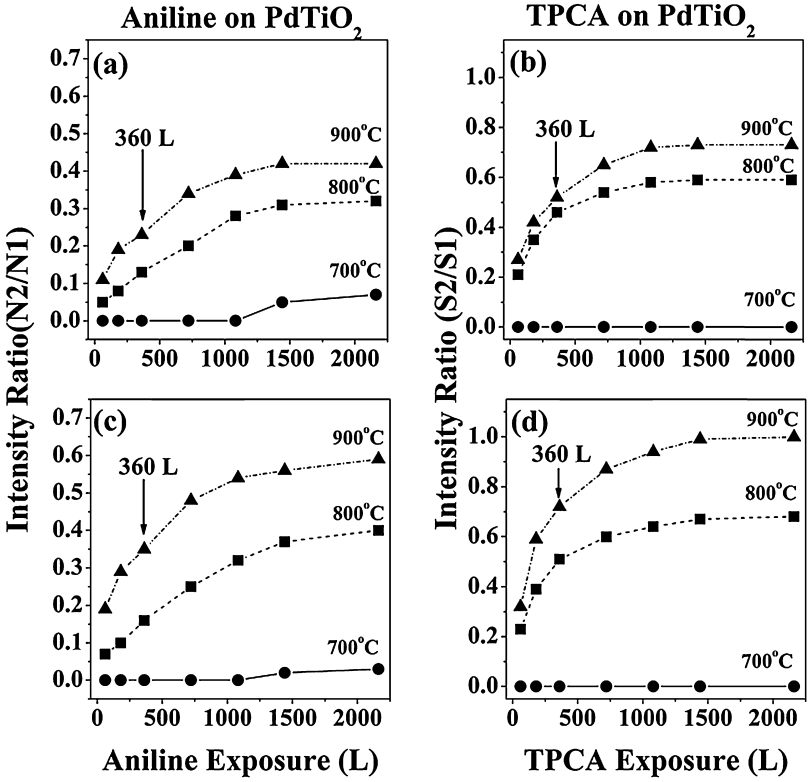

Fig. 6. Plots of the ratios of the intensities of azobenzene (N2) and aniline (N1) (a) and of those of 2-TCA (S2) and TPCA (S1) (b) as functions of molecular exposure under 365 nm UV light. Plots of the ratios of the intensities of azobenzene and aniline (c) and of those of 2-TCA and TPCA (d) as functions of molecular exposure under 540 nm visible light.

Table 1
Ratios of the intensities of azobenzene and aniline and of 2-TCA and TPCA as functions of exposure to aniline and TPCA under 356 nm UV light exposure.

Exposure sample (L)	Azobenzene/aniline			2-TCA/TPCA		
	$PdTiO_2$-700	$PdTiO_2$-800	$PdTiO_2$-900	$PdTiO_2$-700	$PdTiO_2$-800	$PdTiO_2$-900
60	0.00	0.05	0.11	0.00	0.21	0.27
180	0.00	0.08	0.19	0.00	0.35	0.42
360	0.00	0.13	0.23	0.00	0.46	0.52
720	0.00	0.20	0.34	0.00	0.54	0.65
1080	0.00	0.28	0.39	0.00	0.58	0.72
1440	0.05	0.31	0.42	0.00	0.59	0.73
2160	0.00	0.32	0.42	0.00	0.59	0.73

of work function is consisted with the high work function value of PdO (7.9 eV).

We further investigated the dependence of the photocatalytic activities on the light sources, by performing the oxidation under the UV (365 nm) and visible (540 nm) light illumination, respectively, as the exposure of aniline and TPCA changed from 60 to 2160 L (Fig. 6). The illuminated time (or the exposure time) changed from 1 to 36 min. Tables 1 and 2 summarize the variations in the ratios (oxidation capacities) of the intensities of azobenzene and aniline and of those of 2-TCA and TPCA as functions of exposure to aniline and TPCA under 365 nm UV light and 540 nm visible light. Again, the amounts of PdO on the surfaces of the $PdTiO_2$ nanoparticles were positively correlated with the ratio (N2/N1) of the intensities of the azobenzene peak (N2) and the aniline peak (N1) under λ = 365 nm light exposure (Fig. 6a). There was almost no oxidation of aniline on $PdTiO_2$-700; a small amount of azobenzene evolution occurred beyond 1440 L. However, higher N2/N1 intensity ratios were observed with $PdTiO_2$-800 and $PdTiO_2$-900 for all aniline doses. To be more specific, when the surface was exposed to 360 L of aniline, the N2/N1 ratio was 0.23 for $PdTiO_2$-900, which was 1.8 times higher than that of $PdTiO_2$-800 (0.13). A similar trend was observed for TPCA on the $PdTiO_2$ nanoparticles with UV illumination: there was no oxidation on the $PdTiO_2$-700 surface, and the highest S2/S1 intensity ratio (TPCA for S1 and 2-TCA for S2 as marked in Fig. 4) arose for $PdTiO_2$-900.

The variations in the intensity ratios under visible light illumination showed stronger dependence on the post-annealing conditions. For example, after an aniline exposure of 360 L, the N2/N1 intensity ratio for $PdTiO_2$-900 was 0.35, which was 2.2 times higher than that (0.16) for $PdTiO_2$-800 under 540 nm light illumination; in the case of 360 nm light illumination, the intensity ratio was 1.8 times higher for $PdTiO_2$-900 than for $PdTiO_2$-800. For both light sources, $PdTiO_2$-700 exhibits no catalytic activity with respect to aniline oxidation. Similarly, in the case of TPCA oxidation, the difference between the activities of $PdTiO_2$-800 and $PdTiO_2$-900 is higher under visible light.

The different photocatalytic activities between $PdTiO_2$-800 and $PdTiO_2$-900 can be understood in terms of their band gap shifts. Here, λ = 540 nm light was used as the visible light source, which corresponds to an energy of ~2.30 eV according to the relation, E (eV) = 1240 (eV nm)/λ (nm). This energy is close to the $PdTiO_2$-800 band gap of 2.24 eV determined from the valence-band spectrum. Meanwhile, the smaller $PdTiO_2$-900 band gap of 1.92 eV absorbs photons more efficiently under 540 nm visible light exposure, and thus results in larger enhancement on the photo-oxidation activity.

$PdTiO_2$ nanoparticle has an important meaning in terms of the formation of PdO. If the Ti–O–Ti bond weakens, Ti–O bond breaking and oxygen vacancy formation can be facilitated [27]. It has previously been reported that bulk vacancies are less stable than surface vacancies, so oxygen vacancies migrate from the bulk to the surface of TiO_2 [28]. On top of the TiO_2 surface, O atoms combine with neighboring metallic Pd atoms to form PdO. We confirmed that PdO formed on the surfaces of the $PdTiO_2$ samples during annealing at 800 and 900 °C, thus modifying the surface morphology and then the electrons remaining in the oxygen vacancy move toward the neighboring Ti atoms, which are then reduced to form Ti^{3+} cations [29]. The HRPES measurements confirmed the presence of Ti^{3+} cations (Fig. 3) when samples are post-annealed at temperatures above 800 °C. The formation of an oxygen vacancy and the subsequent formation of PdO can be expressed as follows [29]:

$$Ti^{4+}\text{—}O\text{—}Ti^{4+} + Pd \rightarrow Ti^{3+}\text{—}\square\text{—}Ti^{3+} + PdO \quad (1)$$

Therefore, the high-temperature post-annealing treatment of the $PdTiO_2$ nanoparticles is a critical factor in the formation of Ti^{3+} defects and PdO particles on their surfaces. Many previous studies have been demonstrated that Ti^{3+} species and related oxygen vacancies can contribute to improved photocatalytic activity with TiO_2. The photocatalytic activity of TiO_2 can be improved by increasing the light absorption properties, decreasing the photogenerated electron–hole recombination rate, and increasing the catalytic reaction rates with charge carriers on the surface. Ti^{3+} has been reported to influence them to increase the photocatalytic activity of TiO_2 [30,31]. Fig. 5 showed that the light absorption efficiency can be improved with $PdTiO_2$-800 and $PdTiO_2$-900 by extending light absorption to visible light region. Surface defects including Ti^{3+} species and oxygen vacancies can trap the electron or hole to reduce electron–hole recombination rate, and life-time prolonged holes can utilize for oxidation reaction more efficiently. It is also possible that Ti^{3+} species on the surface act as active sites for molecular reactions involving adsorbed chemicals [30]. We conclude that the high catalytic oxidation efficiencies and

Table 2
Ratios of the intensities of azobenzene and aniline and of 2-TCA and TPCA as functions of exposure to aniline and TPCA under 540 nm visible light exposure.

Exposure sample (L)	Azobenzene/aniline			2-TCA/TPCA		
	$PdTiO_2$-700	$PdTiO_2$-800	$PdTiO_2$-900	$PdTiO_2$-700	$PdTiO_2$-800	$PdTiO_2$-900
60	0.00	0.07	0.19	0.00	0.23	0.32
180	0.00	0.10	0.29	0.00	0.39	0.59
360	0.00	0.16	0.35	0.00	0.51	0.72
720	0.00	0.25	0.48	0.00	0.60	0.87
1080	0.00	0.32	0.54	0.00	0.64	0.94
1440	0.02	0.37	0.56	0.00	0.67	0.99
2160	0.03	0.40	0.59	0.00	0.68	1.00

photocatalytic activities of $PdTiO_2$-800 and $PdTiO_2$-900 are due to this increased population of Ti^{3+} defects and PdO on their surfaces.

4. Conclusions

We have demonstrated that PdO and Ti^{3+} was formed on the surfaces of $PdTiO_2$-800 and $PdTiO_2$-900 and that the presence of these species enhances photo-oxidation reactions on those nanoparticle surfaces, which act as catalysts to facilitate the oxidation of aniline to azobenzene and TPCA to 2-TCA. However, neither PdO nor Ti^{3+} form on $PdTiO_2$-700, and so this is inactive with respect to the photo-oxidation of these molecules. We also demonstrated that $PdTiO_2$-800 and $PdTiO_2$-900 exhibited photocatalytic activities by performing oxidation reactions with aniline or TPCA under the visible light exposure because of their reduced band gaps, as determined from their valence-band spectra.

Acknowledgements

This research was supported by the National Research Foundation of Korea (NRF) funded by the Korea government (MSIP) (No. 2014004111 and No. 20090083525). This experiment was supported in part by MSIP and PAL, XFEL project, Korea.

References

[1] A. Fujishima, X. Zhang, D.A. Tryk, Surf. Sci. Rep. 63 (2008) 515–582.
[2] C.L. Pang, R. Lindsay, G. Thorntonb, Chem. Soc. Rev. 37 (2008) 2328–2353.
[3] Y. Du, N.A. Deskins, Z. Zhang, Z. Dohnálek, M. Dupuis, I. Lyubinetsky, Phys. Rev. Lett. 102 (2009) 0961021–0961024.
[4] R. Schaub, E. Wahlström, A. Rønnau, E. Lægsgaard, I. Stensgaard, F. Besenbacher, Science 299 (2003) 377.
[5] S. Livraghi, M.C. Paganini, E. Giamello, A. Selloni, C. Di Valentin, G. Pacchioni, J. Am. Chem. Soc. 128 (2006) 15666.
[6] W.J. Yin, S. Chen, J.H. Yang, X.G. Gong, Y. Yan, S.H. Wei, Appl. Phys. Lett. 96 (2010) 221901.
[7] R. Asahi, T. Morikawa, T. Ohwaki, K. Aoki, Y. Taga, Science 293 (2001) 269–271.
[8] M.H. Ab Rahim, M.M. Forde, R.L. Jenkins, C. Hammond, Q. He, N. Dimitratos, J.A. Lopez-Sanchez, A.F. Carley, S.H. Taylor, D.J. Willock, D.M. Murphy, C.J. Kiely, G.J. Hutchings, Angew. Chem. Int. Ed. Engl. 52 (2013) 1280–1284.
[9] Q. Zhai, S. Xie, W. Fan, Q. Zhang, Y. Wang, W. Deng, Y. Wang, Angew. Chem. Int. Ed. Engl. 52 (2013) 5776–5779.
[10] F. Schreier, J. Quant, Spectrosc. Radiat. Transfer 48 (1992) 743.
[11] L.Z. Mezey, J. Giber, Jpn. J. Appl. Phys. 11 (1982) 1569.
[12] C.D. Terwilliger, Y. Chiang, J. Am. Chem. Soc. 78 (1995) 2045–2055.
[13] G.W. Graham, A.E. O'Neill, D. Uy, W.H. Weber, H. Sun, X.Q. Pan, Catal. Lett. 79 (2002) 1–4.
[14] O. García-Serrano, C. López-Rodriguez, J.A. Andraca-Adame, G. Romero-Paredes, R. Péna-Sierra, Mater. Sci. Eng. B 174 (2010) 273–278.
[15] J.F. Moulder, W.F. Stickle, P.E. Sobol, K.D. Bomben, Handbook of X-ray Photoelectron Spectroscopy, Physical Electronics, Inc, Eden Prairie, MN, 1995.
[16] W.E. Kaden, T. Wu, W.A. Kunkel, S.L. Anderson, Science 326 (2009) 826–830.
[17] K. Roodenko, M. Gensch, J. Rappich, K. Hinrichs, N. Esser, R. Hunger, J. Phys. Chem. B 111 (2007) 7541–7549.
[18] S. Yang, Y. Kim, S. Park, K.-j. Kim, H. Lee, Chem. Asian J. 6 (2011) 2362–2367.
[19] S. Park, S. Yang, N. Shin, E. Lee, H. Lee, J. Phys. Chem. C 114 (2010) 14528–14531.
[20] C.D. Bain, H.A. Biebuyck, G.M. whitesides, Langmuir 5 (1989) 723–727.
[21] G.I.N. Waterhouse, A.K. Wahab, M. Al-Oufi, V. Jovic, D.H. Anjum, D. Sun-Waterhouse, J. Llorca, H. Idriss, Sci. Rep. 3 (2013) 1–5.
[22] A.R. Malagutti, H.A.J.L. Mourão, J.R. Garbin, C. Ribeiro, Appl. Catal. B: Environ. 90 (2009) 205–212.
[23] F. Zuo, L. Wang, T. Wu, Z. Zhang, D. Borchardt, P. Feng, J. Am. Chem. Soc. 132 (2010) 11856–11857.
[24] D.O. Scanlon, C.W. Dunnill, J. Buckeridge, S.A. Shevlin, A.J. Logsdail, S.M. Woodley, C.R.A. Catlow, M.J. Powell, R.G. Palgrave, I.P. Parkin, G.W. Watson, T.W. Keal, P. Sherwood, A. Walsh, A.A. Sokol, Nat. Mater. 12 (2013) 798–801.
[25] R. Schifano, E.V. Monakhov, B.G. Svensson, S. Diplas, Appl. Phys. Lett. 94 (2009) 132101.
[26] E.H. Rhoderick, R.H. Williams, The Metal-Semiconductors Contacts, Oxford University Press, Oxford, 1988.
[27] V. Etacheri, M.K. Seery, S.J. Hinder, S.C. Pillai, Adv. Funct. Mater. 21 (2011) 3744–3752.
[28] K. Jug, N.N. Nair, T. Bredow, Phys. Chem. Chem. Phys. 7 (2005) 2616–2621.
[29] J. Strunk, W.C. Vining, A.T. Bell, J. Phys. Chem. C 114 (2010) 16937–16945.
[30] L.B. Xiong, J.L. Li, B. Yang, Y. Yu, J. Nanomater. (2012) 1–13.
[31] J. Jun, M. Dhayal, J.H. Shin, J.C. Kim, N. Getoff, Radiat. Phys. Chem. 75 (2006) 583–589.